Real-time dynamics of Auger wavepackets and decays in ultrafast charge migration processes
– Supplemental Material –

F. Covito,[1] E. Perfetto,[2,3] A. Rubio,[1,4,5] and G. Stefanucci[3,6]

[1]*Max Planck Institute for the Structure and Dynamics of Matter and Center for Free-Electron Laser Science, Luruper Chaussee 149, 22761 Hamburg, Germany*
[2]*CNR-ISM, Division of Ultrafast Processes in Materials (FLASHit), Area della ricerca di Roma 1, Monterotondo Scalo, Italy*
[3]*Dipartimento di Fisica, Università di Roma Tor Vergata, Via della Ricerca Scientifica, 00133 Rome, Italy*
[4]*Center for Computational Quantum Physics (CCQ), The Flatiron Institute, 162 Fifth avenue, New York NY 10010*
[5]*Nano-Bio Spectroscopy Group, Universidad del País Vasco, 20018 San Sebastian, Spain*
[6]*INFN, Sezione di Roma Tor Vergata, Via della Ricerca Scientifica 1, 00133 Roma, Italy*

(Dated: May 15, 2018)

To distinguish the labels of equations and figures in the Supplemental Material from those of the main text we add "-I" to the latter.

I. DERIVATION OF NEGF EQUATIONS IN HF BASIS

The starting point is the equation of motion for the Green's function $\mathcal{G}(z,z')$ with times z,z' on the Keldysh contour. For the Hamiltonian in Eqs. (1-I) and (2-I) it is convenient to write $\mathcal{G}$ and the correlation self-energy Σ in a block form

$$\mathcal{G}(z,z') = \begin{pmatrix} G(z,z') & \Delta(z,z') \\ \bar{\Delta}(z,z') & C(z,z') \end{pmatrix}, \tag{1}$$

$$\Sigma(z,z') = \begin{pmatrix} \Sigma_G(z,z') & \Sigma_\Delta(z,z') \\ \bar{\Sigma}_\Delta(z,z') & \Sigma_C(z,z') \end{pmatrix}, \tag{2}$$

where G is a matrix with indices in the bound sector, C is a matrix with indices in the continuum sector and Δ, $\bar{\Delta}$ are the off-diagonal blocks. The blocks of the self-energy have the same structure. For the self-energy we make the following approximation

(i) All self-energy diagrams containing Δ or $\bar{\Delta}$ propagators are set to zero (see below for the justification).

From the approximation (i) it follows that $\Sigma_\Delta = \bar{\Sigma}_\Delta = 0$ and that the Hartree-Fock (HF) potential has indices only in the bound sector since the Coulomb integrals in $\hat{H}^{\rm eq}$ have at most one index in the continuum. The explicit form of the HF potential is

$$V_{{\rm HF},ij}(z) = -i\sum_{mn} G_{nm}(z,z^+)w_{imnj}, \tag{3}$$

where $w_{imnj} \equiv 2v_{imnj} - v_{imjn}$.

The equations of motion for the different blocks of $\mathcal{G}$ then read (in matrix form)

$$\left[i\frac{d}{dz} - h_{\rm HF}(z)\right]G(z,z') - (\mathbf{E}(z)\cdot\mathbf{d})\,\bar{\Delta}(z,z') = \delta(z,z') + \int d\bar{z}\;\Sigma_G(z,\bar{z})G(\bar{z},z') \tag{4}$$

$$\left[i\frac{d}{dz} - \mathcal{E}\right]\bar{\Delta}(z,z') - (\mathbf{E}(z)\cdot\mathbf{d})\,G(z,z') = \delta(z,z') + \int d\bar{z}\;\Sigma_C(z,\bar{z})\bar{\Delta}(\bar{z},z') \tag{5}$$

$$\left[i\frac{d}{dz} - \mathcal{E}\right]C(z,z') = \delta(z,z') + \int d\bar{z}\;\Sigma_C(z,\bar{z})C(\bar{z},z') \tag{6}$$

where in Eq. (4) we have defined the nonequilibrium single-particle HF Hamiltonian

$$h_{\rm HF} = h + V_{\rm HF} + \mathbf{E}\cdot\mathbf{d}, \tag{7}$$

and in the last two equations we have defined the matrix $\mathcal{E}_{\mu\nu} = \delta_{\mu\nu}\epsilon_\mu$. The blocks of the dipole matrix are unambiguously determined by the contractions and we do therefore use the same symbol for all four blocks. Notice that no coupling with the electric field appears in Eq. (6) since we set $\mathbf{d}_{\mu\mu'} = 0$ in Eq. (2-I).

Next we observe that if the energy-window of the photoelectron does not overlap with that of the Auger electron then we can make the approximation:

(ii) $\Sigma_C(z,\bar{z})\bar{\Delta}(\bar{z},z') \simeq 0$.

With the approximation (ii) we easily integrate Eq. (5) and obtain

$$\bar{\Delta}_{\mu j}(z,z') = \sum_n \int d\bar{z}\; C^0_\mu(z,\bar{z})\,(\mathbf{E}(\bar{z})\cdot\mathbf{d}_{\mu n})\,G_{nj}(\bar{z},z'), \tag{8}$$

where C^0 is the solution of Eq. (6) with $\Sigma_C = 0$. Since $\mathcal{E}$ is diagonal so is C^0.

Inserting Eq. (8) into Eq. (4) we get

$$\left[i\frac{d}{dz} - h_{\rm HF}(z)\right]G(z,z') = \delta(z,z') + \int d\bar{z}\,[\Sigma_G(z,\bar{z}) + \Sigma_{\rm ion}(z,\bar{z})]\,G(\bar{z},z'), \tag{9}$$

where we have defined the ionization self-energy

$$\Sigma_{{\rm ion},ij}(z,\bar{z}) \equiv \sum_\mu (\mathbf{E}(z)\cdot\mathbf{d}_{i\mu})\,C^0_\mu(z,\bar{z})\,(\mathbf{E}(\bar{z})\cdot\mathbf{d}_{\mu j})\,. \tag{10}$$

The diagrammatic representation of the ionization self-energy is displayed in the bottom diagram of Fig. 1(b)-I where, to avoid a proliferation of different symbols, we used G^0_μ instead of C^0_μ (in the main text we also used $G_{\mu\nu}$ instead of $C_{\mu\nu}$). Notice that $\Sigma_{\rm ion}$ vanishes for times at which the external pulse is zero.

We now have to specify the approximation for the correlation self-energy. For weakly interacting closed systems (no continuum states) the self-consistent second-Born approximation (2B) has been shown to be accurate in several nonequilibrium situations [1–10]. The very same approximation describes Auger scatterings provided that we also consider interaction lines with one index in the continuum [11, 12]. We therefore approximate Σ_G and Σ_C as the sum of the 2B diagrams. It is easy to show that for a $\mathcal{G}$ initially block diagonal (no electrons in the continuum in the ground state) the off-diagonal blocks remain zero for all times in the 2B approximation. This justifies the approximation (i).

The 2B diagrams for Σ_G can be split into diagrams with interaction lines having all indices in the bound sector (v) and diagrams with interaction lines having one index in the continuum sector (v^A):

$$\Sigma_G = \Sigma_{\rm c} + \Sigma_{\rm Auger}. \tag{11}$$

Using the Feynman rules, see top and middle panel of Fig. 1, one finds

$$\Sigma_{{\rm c},ij}(z,z') = \sum_{mn,pq,sr} v_{irpm}w_{nqsj} \times G_{mn}(z,z')G_{pq}(z,z')G_{sr}(z',z), \tag{12}$$

and

$$\Sigma_{{\rm Auger},ij}(z,z') = \sum_{mn\,pq}\sum_\mu G_{mn}(z,z') \times \big[C_{\mu\nu}(z,z')G_{pq}(z',z)(v^A_{iqm\mu}w^A_{\nu npj} + v^A_{iq\mu m}w^A_{\nu pj}) + G_{pq}(z,z')C_{\mu\nu}(z',z)v^A_{i\nu pm}w^A_{nq\mu j}\big]\,. \tag{13}$$

The correlation self-energy $\Sigma_{\rm c}$ is also given in the top diagram of Fig. 1(b)-I.

The 2B diagrams for Σ_C do instead contain only v^A interaction lines since both indices of Σ_C are in the continuum sector. From the bottom diagram of Fig. 1 one finds

$$\Sigma_{C,\mu\nu}(z,z') = \sum_{mn,pq,sr} v^A_{\mu rpm}w^A_{nqs\nu} \times G_{mn}(z,z')G_{pq}(z,z')G_{sr}(z',z). \tag{14}$$

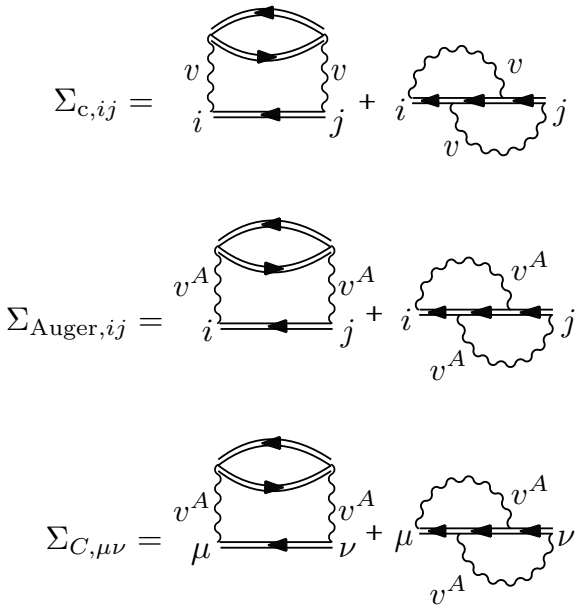

FIG. 1: Self-energy diagrams with indices in the bound sector for intramolecular scattering (top) and Auger scattering (middle). Self-energy diagrams for Auger electrons (bottom).

For a short and weak laser pulse the off-diagonal matrix elements of C are small. We therefore make the approximation

(iii) $C_{\mu\nu} \simeq \delta_{\mu\nu}C_\mu$ in $\Sigma_{\rm Auger}$

Implementing (iii) in Eq. (13) and extracting the lesser/greater component we get precisely the self-energy in Eq. (5-I).

To summarize, with the approximations (i-iii) the equations of motion become

$$\left[i\frac{d}{dz} - h_{\rm HF}(z)\right]G(z,z') = \delta(z,z') + \int d\bar{z}\,\Sigma(z,\bar{z})G(\bar{z},z') \tag{15}$$

$$\left[i\frac{d}{dz} - \mathcal{E}\right]C(z,z') = \delta(z,z') + \int d\bar{z}\,\Sigma_C(z,\bar{z})C(\bar{z},z') \tag{16}$$

where in Eq. (15) we have defined

$$\Sigma \equiv \Sigma_{\rm c} + \Sigma_{\rm ion} + \Sigma_{\rm Auger}. \tag{17}$$

Taking the adjoint of Eqs. (15,16), summing the resulting equations to Eqs. (15,16) and evaluating the result in $z = z^+ = t$ we get the equation of motion for

the density matrices $\rho_{ij}(t) = -iG_{ij}(z, z^+)$ and $f_{\mu\nu}(t) = -iC_{\mu\nu}(z, z^+)$:

$$\dot\rho = -i\left[h_{\rm HF}, \rho\right] - \mathcal{I} - \mathcal{I}^\dagger, \tag{18}$$

$$\dot f_{\mu\nu} = -i(\epsilon_\mu - \epsilon_\nu) f_{\mu\nu} - \mathcal{J}_{\mu\nu} - \mathcal{J}^*_{\nu\mu}, \tag{19}$$

where

$$\mathcal{I}(t) = \int_0^t d\bar t \big[\Sigma^>(t,\bar t)G^<(\bar t, t) - \Sigma^<(t,\bar t)G^>(\bar t, t)\big], \tag{20}$$

$$\mathcal{J}(t) = \int_0^t d\bar t \big[\Sigma^>_C(t,\bar t)C^<(\bar t, t) - \Sigma^<_C(t,\bar t)C^>(\bar t, t)\big]. \tag{21}$$

Equations (18,19) do not close on ρ and f since the right hand side depends on G and C calculated at different times. To close the equations we make the Generalized Kadanoff-Baym Ansatz [13] (GKBA). According to the GKBA we can replace all $G^{\lessgtr}$ and $C^{\lessgtr}$ appearing in $\mathcal{I}$ and $\mathcal{J}$ with

$$G^{\lessgtr}(t,\bar t) = \mp\left[G^{\rm R}(t,t')\rho^{\lessgtr}(t') - \rho^{\lessgtr}(t)G^{\rm A}(t,t')\right], \tag{22}$$

$$C^{\lessgtr}(t,\bar t) = \mp\left[C^{\rm R}(t,t')f^{\lessgtr}(t') - f^{\lessgtr}(t)C^{\rm A}(t,t')\right], \tag{23}$$

where $\rho^< = \rho$, $\rho^> = 1-\rho$ and similarly $f^< = f$, $f^> = 1-f$. For the retarded/advanced Green's function we consider the HF approximation according to which

$$G^{\rm R}(t,t') = [G^{\rm A}(t',t)]^\dagger = -i\theta(t-t')\mathcal{T}\left[e^{-i\int_{t'}^t d\bar t\, h_{\rm HF}(\bar t)}\right], \tag{24}$$

$$C^{\rm R}_{\mu\nu}(t,t') = [C^{\rm A}_{\nu\mu}(t',t)]^* = -i\delta_{\mu\nu}\theta(t-t')e^{-i\epsilon_\mu(t-t')}. \tag{25}$$

Since $h_{\rm HF}$ is a functional of ρ we see that Eqs. (18,19) become nonlinear integro-differential equations for $\rho_{ij}(t)$ and $f_{\mu\nu}(t)$. Notice also that in the equation for ρ the dependence on f is only through the diagonal elements $f_\mu \equiv f_{\mu\mu}$ appearing in $\Sigma_{\rm Auger}$, due to the approximation (iii). If we set $\mu = \nu$ in Eq. (19) then for the right hand side to depend only on f_μ we have to make the approximation

(iv) $f_{\mu\nu} = \delta_{\mu\nu} f_\mu$ in $\mathcal{J}$

which is consistent with the approximation (iii).

It is easy to show that in this way the equation for ρ becomes the first of Eqs. (4-I) and that the equation for $f_{\mu\nu}$ becomes Eq. (9-I), which for $\mu = \nu$ reduces to the second of Eqs. (4-I).

II. NEGF@GRID VERSUS COUPLED NEGF CALCULATIONS

To assess the accuracy of the approximations made at the level of the Hamiltonian with Eqs. (1-I,2-I) and at the level of NEGF with (i-iv), we considered a 1D atom on a grid. In the grid basis the total Hamiltonian in second quantization reads

$$\begin{aligned}\hat H(t) &= \sum_{\substack{mn\\ \sigma}} \psi^\dagger_\sigma(x_m) h(x_m,x_n)\psi_\sigma(x_n) \\ &+ \frac{1}{2}\sum_{\substack{mn\\ \sigma\sigma'}} \psi^\dagger_\sigma(x_m)\psi^\dagger_{\sigma'}(x_n) v(x_m,x_n)\psi_{\sigma'}(x_n)\psi_\sigma(x_m) \\ &+ E(t)\sum_{\substack{m\\ \sigma}} x_m \psi^\dagger_\sigma(x_m)\psi_\sigma(x_m).\end{aligned} \tag{26}$$

where the one-particle Hamiltonian $h(x,x')$ and the interaction $v(x,x')$ are defined in the main text. The equation of motion for the density matrix in grid basis $\rho(x_m,x_n,t) = G(x_m,z;x_n,z^+)$ in the 2B approximation is

$$\begin{aligned}\dot\rho(x_m,x_n,t) = -i\sum_p &[h_{\rm HF}(x_m,x_p,t)\rho(x_p,x_n,t) \\ &-\rho(x_m,x_p,t)h_{\rm HF}(x_p,x_n,t)] \\ &-\mathcal{I}_g(x_m,x_n,t) - \mathcal{I}^*_g(x_n,x_m,t).\end{aligned} \tag{27}$$

In Eq. (27) we have the HF Hamiltonian in grid basis

$$h_{\rm HF}(x_m,x_p,t) = h(x_m,x_p) + V_{\rm HF}(x_m,x_p,t) + \delta_{mp}E(t)x_m, \tag{28}$$

with HF potential

$$\begin{aligned}V_{\rm HF}(x_m,x_p,t) &= 2\delta_{nm}\sum_q v(x_m,x_q)\rho(x_q,x_q,t) \\ &- v(x_m,x_p)\rho(x_m,x_p,t),\end{aligned} \tag{29}$$

and the collision integral in grid basis

$$\begin{aligned}\mathcal{I}_g(x_m,x_n,t) = \sum_p \int_0^t d\bar t\big[&\Sigma^>_g(x_m,t;x_p,\bar t)G^<(x_p,\bar t;x_n,t) \\ &\Sigma^<_g(x_m,t;x_p,\bar t)G^>(x_p,\bar t;x_n,t)\big],\end{aligned} \tag{30}$$

with the 2B self-energy

$$\begin{aligned}\Sigma^{\lessgtr}_g(x_m,t;x_p,\bar t) &= \sum_{rs} v(x_m,x_r)v(x_p,x_s) \\ \times\Big[&2G^{\lessgtr}(x_m,t;x_p,\bar t)G^{\lessgtr}(x_r,t;x_s,\bar t)G^{\gtrless}(x_s,\bar t;x_r,t) \\ &- G^{\lessgtr}(x_m,t;x_s,\bar t)G^{\gtrless}(x_s,\bar t;x_r,t)G^{\lessgtr}(x_r,t;x_p,\bar t)\Big].\end{aligned} \tag{31}$$

The NEGF@grid results have been obtained by solving Eq. (27) with lesser/greater Green's function evaluated at the GKBA level. Except that for the 2B approximation

to Σ_g, no other approximation has been made. For a system with $N_{\rm grid}$ points this require to propagate and store matrices $N_{\rm grid} \times N_{\rm grid}$.

In order to apply the coupled NEGF scheme based on Eqs. (4-I) we first solve the self-consistent HF problem and extract the equilibrium bound eigenfunctions $\varphi_i(x_n)$ and continuum eigenfunctions $\varphi_\mu(x_n)$ of energy ϵ_i and ϵ_μ respectively. The HF eigenfunctions are then used to calculate the matrix elements in the bound sector of the one-particle Hamiltonian

$$h_{ij} = \sum_{mn} \varphi_i^*(x_m) h(x_m, x_n) \varphi_j(x_m), \tag{32}$$

the dipole operator

$$d_{ij} = \sum_{m} \varphi_i^*(x_m) x_m \varphi_j(x_m), \tag{33}$$

and the Coulomb repulsion

$$v_{ijpq} = \sum_{mn} \varphi_i^*(x_m) \varphi_j^*(x_n) v(x_m, x_n) \varphi_p(x_n) \varphi_q(x_m). \tag{34}$$

The continuum HF eigenfunctions are used to calculate the bound-continuum matrix elements of the dipole operator

$$d_{i\mu} = \sum_{m} \varphi_i^*(x_m) x_m \varphi_\mu(x_m), \tag{35}$$

and the Coulomb repulsion responsible for Auger scatterings

$$v^A_{ijp\mu} = \sum_{mn} \varphi_i^*(x_m) \varphi_j^*(x_n) v(x_m, x_n) \varphi_p(x_n) \varphi_\mu(x_m). \tag{36}$$

With this information we approximate the original Hamiltonian in Eq. (26) in accordance with Eqs. (1-I,2-I), i.e.,

$$\begin{aligned} \hat{H}(t) = & \sum_{\substack{ij \\ \sigma}} h_{ij} \hat{c}^\dagger_{i\sigma} \hat{c}_{j\sigma} + \frac{1}{2} \sum_{\substack{ijpq \\ \sigma\sigma'}} v_{ijpq} \hat{c}^\dagger_{i\sigma} \hat{c}^\dagger_{j\sigma'} \hat{c}_{p\sigma'} \hat{c}_{q\sigma} \\ & + \sum_{\mu\sigma} \epsilon_\mu \hat{c}^\dagger_{\mu\sigma} \hat{c}_{\mu\sigma} + \sum_{\substack{ijp\mu \\ \sigma\sigma'}} v^A_{ijp\mu} \left(\hat{c}^\dagger_{i\sigma} \hat{c}^\dagger_{j\sigma'} \hat{c}_{p\sigma'} \hat{c}_{\mu\sigma} + \text{h.c.} \right) \\ & + E(t) \sum_{\substack{ij \\ \sigma}} d_{ij} \hat{c}^\dagger_{i\sigma} \hat{c}_{j\sigma} + E(t) \sum_{\substack{i\mu \\ \sigma}} \left(d_{i\mu} \hat{c}^\dagger_{i\sigma} \hat{c}_{\mu\sigma} + \text{h.c.} \right), \end{aligned} \tag{37}$$

where $\hat{c}_{i\sigma}$ ($\hat{c}_{\mu\sigma}$) are annihilation operators for an electron in the HF orbital φ_i (φ_μ) with spin σ. Of course, had we included in Eq. (37) the off-diagonal one-electron terms containing $h_{i\mu}$, $h_{\mu\mu'}$ and $d_{\mu\mu'}$ and the interaction terms containing $v_{ij\mu\mu'}$, $v_{i\nu\mu\mu'}$ and $v_{\nu'\nu\mu\mu'}$ we would have got the same Hamiltonian as in Eq. (26) but in the HF basis.

With the approximate Hamiltonian in Eq. (37) we solve the coupled NEGF equations (4-I) which, we emphasize again, have been derived by making the additional approximations (i-iv) of the previous section. The agreement between the full-grid simulations and the simulations based on Eqs. (4-I) indicate that the latter are enough to capture qualitatively and quantitatively the physics of the Auger decay.

We observe that in the grid simulations the self-energy Σ_g contains all possible scatterings, including those contained in the self-energies $\Sigma_{\rm c}$ and $\Sigma_{\rm Auger}$ of the coupled NEGF scheme. Furthermore, in the grid simulations no ionization self-energy appears since the photoionization is accounted for by explicitly including all grid points (even those far away from the nucleus). In other words, *all* elements $\rho(x_m, x_n, t)$ are coupled and propagated in time.

III. CI VERSUS COUPLED NEGF CALCULATIONS

To further check the quality of the NEGF Eqs. (4-I) we have also solved the time-dependent problem using a Configuration Interaction (CI) expansion.

The neutral 1D atom described in the main text of the paper has four electrons, two in the core and two in the valence levels. We are interested in suddenly removing a core electron of, say, spin down, and in studying how the system evolves with the Hamiltonian in Eq. (37). For the CI expansion we use the following three-body states

$$|\Phi_x\rangle = \hat{c}^\dagger_{c\uparrow} \hat{c}^\dagger_{v\downarrow} \hat{c}^\dagger_{v\uparrow} |0\rangle, \tag{38}$$

$$|\Phi_g\rangle = \hat{c}^\dagger_{c\uparrow} \hat{c}^\dagger_{c\downarrow} \hat{c}^\dagger_{v\uparrow} |0\rangle, \tag{39}$$

$$|\Phi_\mu\rangle = \hat{c}^\dagger_{c\uparrow} \hat{c}^\dagger_{c\downarrow} \hat{c}^\dagger_{\mu\uparrow} |0\rangle, \tag{40}$$

describing the initially photoionized state (Φ_x), the cationic ground state (Φ_g) and the Auger states (Φ_μ). We expand the state of the system at time t according to

$$|\Psi(t)\rangle = a_x(t)|\Phi_x\rangle + a_g(t)|\Phi_g\rangle + \sum_\mu a_\mu(t)|\Phi_\mu\rangle, \tag{41}$$

and impose the initial condition $a_x(0) = 1$ and $a_g(0) = a_\mu(0) = 0$. Using the fact that in the HF basis $h_{\rm HF}$ is diagonal, it is easy to show that the cationic ground state decouples and the dynamics is governed by the equations below

$$i\dot{a}_x = E_x a_x + \sum_\mu v_{c\mu vv} a_\mu, \tag{42}$$

$$i\dot{a}_\mu = v_{c\mu vv} a_x + E_\mu a_\mu. \tag{43}$$

The three-body energies are

$$E_x = 2\epsilon_v + \epsilon_c - v_{cccc} - 4v_{cvvc} + 2v_{cvcv} - v_{vvvv}, \tag{44}$$

$$E_\mu = \epsilon_\mu + 2\epsilon_c - v_{cccc} - 4v_{cvvc} + 2v_{cvcv}, \tag{45}$$

where the HF energies of the core and valence levels are given by

$$\epsilon_c = h_{cc} + v_{cccc} + 2v_{cvvc} - v_{cvcv}, \tag{46}$$

$$\epsilon_v = h_{vv} + v_{vvvv} + 2v_{vccv} - v_{vcvc}. \tag{47}$$

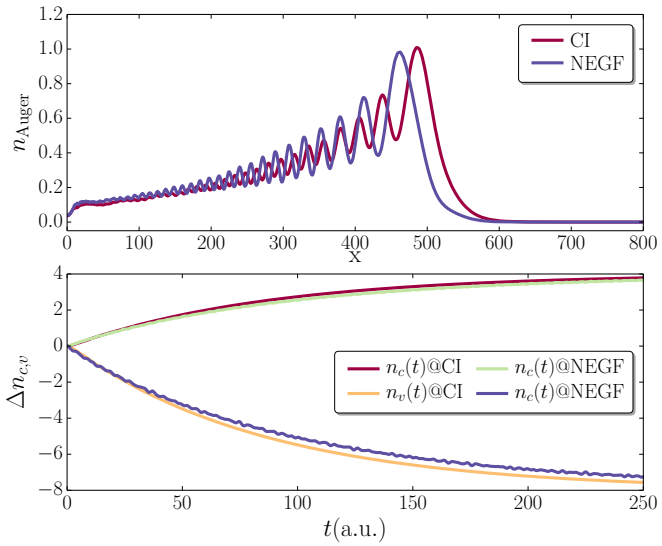

FIG. 2: Auger wavepacket (top) and variation of the occupations of the core and valence levels (bottom) in CI and in coupled NEGF. Same parameters as in top panel of Fig. 4-I.

The energy $\epsilon_{\rm Auger} = \epsilon_{\mu_A}$ of the Auger electron is determined by the condition $E_{\mu_A} = E_x$ which yields

$$\epsilon_{\rm Auger} = 2\epsilon_v - \epsilon_c - v_{vvvv} \tag{48}$$

as it should. The red-shift v_{vvvv} is due to the repulsion of the two holes in the final state. In order to capture this red-shift using Many-Body Perturbation Theory (MBPT) one should go beyond the 2B approximation for the self-energy and consider the T-matrix approximation in the particle-particle sector [14, 15]. We observe, however, that for weakly correlated molecules, like organic molecules and biomolecules, the magnitude of the valence-valence repulsion is typically less than 1 eV; hence, neglecting this repulsion does not substantially affect the dynamics during the first ten of femtoseconds or so.

For the 1D atom the valence-valence repulsion is mainly responsible for reducing the speed of the Auger electron. The form of the Auger wavepacket as well as the time-dependent behavior of the refilling of the core-hole are not altered if we set $v_{vvvv} = 0$ in Eq. (44). For a fair comparison with the coupled NEGF Eqs. (4-I) we therefore solve Eqs. (42,43) using $E_x^{2B} = E_x + v_{vvvv}$ in place of E_x. In Fig. 2 we compare the Auger wavepacket (top panel) and the occupation of the core and valence levels (bottom panels) calculated using CI and the coupled NEGF equations (4-I). Also in this case the agreement is rather satisfactory.

The analytic calculation can be carried on further if we assume that the broadening

$$\Gamma(\omega) = 2\pi \sum_\mu |v_{c\mu vv}|^2 \delta(\omega - \epsilon_\mu) \tag{49}$$

is a weakly dependent function of ω for $\omega \simeq \epsilon_{\rm Auger}$. In this case it is straightforward to show that the amplitudes

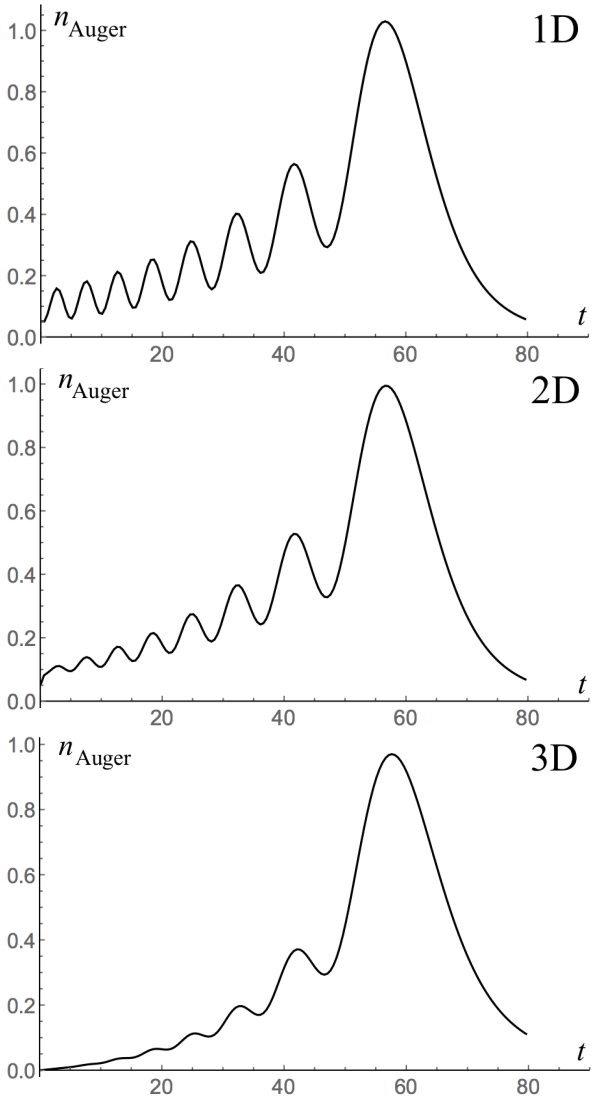

FIG. 3: Auger wavepacket (in arbitrary units) for $\Gamma = 0.05$ and $\epsilon_{\rm Auger} = 1$ after a time $t = 50$ from the sudden removal of a core electron. Top: $n_{\rm Auger}(r,t)$ in 1D. Middle: $rn_{\rm Auger}(r,t)$ in 2D. Bottom: $r^2 n_{\rm Auger}(r,t)$ in 3D.

a_μ are given by

$$a_\mu(t) = -v_{c\mu vv} e^{-iE_\mu t}\, \frac{e^{i(\epsilon_\mu - \epsilon_{\rm Auger} + i\Gamma/2)t} - 1}{\epsilon_\mu - \epsilon_{\rm Auger} + i\Gamma/2} \tag{50}$$

which coincides with Eq. (11-I). The occurrence of ripples on the tail of the Auger wavepacket stems from the structure of the a_μ's. In fact, the ripples are independent of the dimension of the system and of the details of the continuum states in the vicinity of the nucleus. As an example, let $\mu = \mathbf{p}$ be the momentum in D dimension and let us use planewaves $\varphi_\mu(\mathbf{r}) = \varphi_{\mathbf{p}}(\mathbf{r}) = e^{i\mathbf{p}\cdot\mathbf{r}}$ for the continuum states. We further consider a free dispersion $\epsilon_\mu = \epsilon_{\mathbf{p}} = p^2/2$ and, for simplicity, an Auger interaction $v_{c\mu vv} = v_{c\mathbf{p}vv}$ independent of $\mathbf{p}$ so that $a_\mu = a_p$ depends only on the modulus $p = |\mathbf{p}|$ of the momentum,

see Eq. (50). Then, the Auger wavepacket is spherically symmetric and its density is given by

$$n_{\rm Auger}(r,t) = \left| \int \frac{d^D p}{(2\pi)^D} a_p(t) e^{i\mathbf{p}\cdot\mathbf{r}} \right|^2 . \qquad (51)$$

In Fig. 3 we show $n_{\rm Auger}(r,t)$ for $\Gamma = 0.05$ and an Auger energy $\epsilon_{\rm Auger} = 1$ after a time $t = 50$ from the sudden removal of the core electron. The figure shows $n_{\rm Auger}(r,t)$ in 1D (top), $r n_{\rm Auger}(r,t)$ in 2D (middle) and $r^2 n_{\rm Auger}(r,t)$ in 3D (bottom). In all cases we appreciate the occurrence of ripples although they tend to get smeared out as the dimension increases.

IV. DESCRIPTION OF ANIMATIONS

The animation continuum_occupations.mp4 shows the evolution of the occupations f_μ of the continuum HF states for the 1D atom driven by the external laser pulse of Eq. (8-I). Same parameters as in the bottom panel of Fig. (2-I).

The animation Auger_wavepacket.mp4 shows the evolution of the Auger wavepacket as obtained by solving first Eqs.(4-I) and then Eq. (9-I). Same parameters as in the top panel of Fig. 4-I.

[1] K. Balzer, S. Bauch, and M. Bonitz, Phys. Rev. A **82**, 033427 (2010), URL https://link.aps.org/doi/10.1103/PhysRevA.82.033427.

[2] K. Balzer, S. Hermanns, and M. Bonitz, EPL (Europhysics Letters) **98**, 67002 (2012), URL http://stacks.iop.org/0295-5075/98/i=6/a=67002.

[3] N. Säkkinen, M. Manninen, and R. van Leeuwen, New Journal of Physics **14**, 013032 (2012), URL http://stacks.iop.org/1367-2630/14/i=1/a=013032.

[4] S. Hermanns, N. Schlünzen, and M. Bonitz, Phys. Rev. B **90**, 125111 (2014), URL https://link.aps.org/doi/10.1103/PhysRevB.90.125111.

[5] N. Schlünzen and M. Bonitz, Contrib. Plasma Phys. **56**, 5 (2016), ISSN 1521-3986, URL http://dx.doi.org/10.1002/ctpp.201610003.

[6] M. Hopjan, D. Karlsson, S. Ydman, C. Verdozzi, and C.-O. Almbladh, Phys. Rev. Lett. **116**, 236402 (2016), URL https://link.aps.org/doi/10.1103/PhysRevLett.116.236402.

[7] Y. B. Lev and D. R. Reichman, EPL (Europhysics Letters) **113**, 46001 (2016), URL http://stacks.iop.org/0295-5075/113/i=4/a=46001.

[8] N. Schlünzen, J.-P. Joost, F. Heidrich-Meisner, and M. Bonitz, Phys. Rev. B **95**, 165139 (2017), URL https://link.aps.org/doi/10.1103/PhysRevB.95.165139.

[9] A.-M. Uimonen, E. Khosravi, A. Stan, G. Stefanucci, S. Kurth, R. van Leeuwen, and E.K.U. Gross, Phys. Rev. B **84**, 115103 (2011).

[10] E. V. Boström, A. Mikkelsen, C. Verdozzi, E. Perfetto, and G. Stefanucci, Nano Lett. **18**, 785 (2018), https://doi.org/10.1021/acs.nanolett.7b03995, URL https://doi.org/10.1021/acs.nanolett.7b03995.

[11] C.-O. Almbladh, A. L. Morales, and G. Grossmann, Phys. Rev. B **39**, 3489 (1989), URL https://link.aps.org/doi/10.1103/PhysRevB.39.3489.

[12] C.-O. Almbladh and A. L. Morales, Phys. Rev. B **39**, 3503 (1989), URL https://link.aps.org/doi/10.1103/PhysRevB.39.3503.

[13] P. Lipavský, V. Špička, and B. Velický, Phys. Rev. B **34**, 6933 (1986), URL https://link.aps.org/doi/10.1103/PhysRevB.34.6933.

[14] M. Cini, Solid state communications **88**, 1101 (1993).

[15] G. A. Sawatzky, Phys. Rev. Lett. **39**, 504 (1977), URL https://link.aps.org/doi/10.1103/PhysRevLett.39.504.